PATIENT-SPECIFIC FINITE-ELEMENT SIMULATION OF RESPIRATORY MECHANICS FOR RADIOTHERAPY GUIDANCE, A FIRST EVALUATION STUDY

B. Fuerst[1,2]*, T. Mansi*[2]*, P. Khurd*[2]*, J. Zhang*[2]*, J. Declerck*[3]*, T. Boettger*[4]*, N. Navab*[5]*, J. Bayouth*[6] *and A. Kamen*[2]

[1] Technische Universität München, Munich, Germany
[2] Siemens Corporation, Corporate Research and Technology, Image Analytics and Informatics, Princeton, NJ
[3] Siemens Molecular Imaging, Oxford, UK
[4] Siemens Radiation Oncology, Heidelberg, Germany
[5] Technische Universität München, Computer Aided Medical Procedures, Munich, Germany
[6] Iowa University, Radiation Oncology, USA

ABSTRACT

During radiotherapy of lung tumors, the respiratory motion must be tracked to reduce radiation of healthy tissue. This is usually done by using a respiratory surrogate, but with limited accuracy. We investigate how patient-specific finite element models (FEM) of respiratory mechanics can predict the motion of the lungs. First, the anatomical models of the lungs and thorax are extracted from CT images automatically. Then, a biomechanical model is used to simulate the respiratory motion based on a novel thorax/lung interaction force that simulates the pleural cavity. Our model is not driven by image forces but by thoracic pressures personalized using a multivariate optimizer. The proposed model is validated on three DIR-Lab datasets, yielding a promising internal landmark error of $3.33 \pm 0.60\,mm$. Our model may represent a tool for lung deformation prediction and therapy guidance.

Index Terms— Lung / Thorax FEM, Respiratory Mechanics, Trust-Region Optimization, Pressure Estimation

1. INTRODUCTION

Radiotherapy is an effective treatment for lung tumors. During interventions, malignant cells are killed using focused ionized rays [1]. To avoid destroying healthy tissue, the tumor needs to be tracked while patient is breathing. 4D Computed Tomography (CT) is the modality of choice for radiotherapy planning as it allows analysis of the respiratory patterns. However, due to radiation, CT cannot be employed continuously during the treatment. As a result, no 4D information is available during intervention. Lung motion is estimated based on surrogate signals, like a spirometer, abdominal pressure belt or external markers, resulting in a sub-optimal tumor localization due to the non-linear relationship between the surrogate and the complex 3D deformation.

In the last decade, several approaches have been proposed to estimate the patient-specific spatio-temporal patterns of the respiratory movements. These can be classified into two categories: image-based and computational-biomechanical methods. On the one hand, image-based methods estimate the lung deformations between two phases of the respiratory cycle using non-linear image registration. Rietzel *et al.* [2] estimated a respiratory motion model from 4D CT using Free-Form Deformation to determine the maximal displacement of the tumor. Ehrhardt *et al.* [3] created a lung-motion atlas from a population of patients. Although such an atlas could be used as a first approximation of the respiration motion of a patient, its generalization to different respiratory patterns, under different condition, is not straightforward. A solution would be to adapt the motion atlas to the patient or to guide the patient's breathing [4], but a long duration can cause patient discomfort and increase the error rate. Computational-biomechanical approaches rely on FEM of the lung physiology to simulate its deformation during respiration [5, 6]. A volumetric model of the lung anatomy is created from patient images. Then, the model is deformed according to body forces, which simulate the biomechanics of the lung, and surface loadings, to deform the organ throughout the respiratory cycle. In [5, 6], the surface load and deformation is limited by a second geometry extracted from a different phase (e.g. EI to EE), thus relying on 4D image data [7, 8]. Therefore such models can still not be used during intervention where no or only one phase is available.

Our overarching goal is to develop a generative model that can predict patient respiratory motion under different conditions using imaging data acquired prior to the intervention and intra-operative surrogate signals. We investigate a patient-specific FEM of the lungs and thorax to simulate respiratory mechanics. According to the physiological process, we propose to apply pressure forces to the thoracic cavity instead of manipulating the lungs directly (Sec. 2). Generated thoracic stresses are then transferred to the lungs through a novel model of the pleural cavity. Another contribution of this study

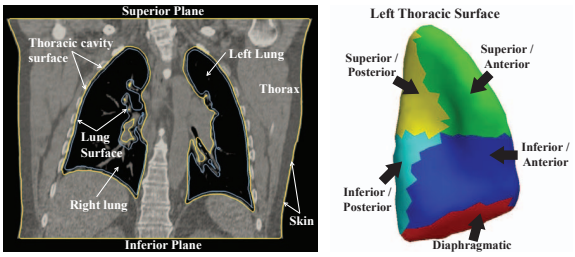


Fig. 1. *Left panel*: Coronal slice showing thorax (*yellow*) and lungs (*blue*) segmentations. *Right panel*: Surface zones for regional personalization.

is the automatic estimation of the required forces to load the lung from End of Expiration (EE) to End of Inspiration (EI) using a trust-region algorithm. Expiration is simulated by turning off the pressures. The model is validated on three DIR-Lab datasets (Sec. 3). Manually annotated landmarks are moved according to simulated deformations and compared with the ground truth. Sec. 4 concludes the paper.

2. METHODS

Our approach consists of three main stages. First, an accurate anatomical model of patient's lung and thorax is automatically generated from CT images (Sec. 2.1). This model is then used to simulate respiratory motion, driven by a thoracic pressure field (Sec. 2.2). A trust-region optimizer is employed to estimate the pressure loading required to deform the lung from EE to EI, which allows personalization of applied force and compensation for varying material properties (Sec. 2.3).

2.1. Anatomical Model of Lung and Thorax

The first step is to create an anatomical model of patient's thorax and lungs (airways are not considered in this study). It is achieved automatically, under expert guidance, using a machine learning segmentation with level-set optimization previously described in [9]. The two lungs are not connected and the thorax model has three surfaces: outer surface (skin, superior and inferior planes) and two inner thoracic cavities (Fig. 1, left panel). Next, tetrahedral meshes of the thorax and the lungs are computed[1]. Finally, each thoracic cavity surface is subdivided into five zones for regional personalization of the thoracic pressure (see Fig. 1, right panel).

2.2. FE Model of Lung/Thorax interactions

The respiratory motion is simulated by solving simultaneously the dynamics equations for the lungs and the thorax:

$$\begin{aligned} \mathrm{M}^l\ddot{\mathbf{U}}^l + \mathrm{C}^l\dot{\mathbf{U}}^l + \mathrm{K}^l\mathbf{U}^l &= \mathbf{F}_c^{t\to l} \\ \mathrm{M}^t\ddot{\mathbf{U}}^t + \mathrm{C}^t\dot{\mathbf{U}}^t + \mathrm{K}^t\mathbf{U}^t &= \mathbf{F}_c^{l\to t} + \mathbf{F}_p \end{aligned} \quad (1)$$

The superscripts l and t stand for *lung* and *thorax* respectively. $\mathrm{M}^{\{l,t\}}$ are the lumped mass matrices (mass densities: $\rho^l = 1.05\,g/mL$, $\rho^t = 1.50\,g/mL$), $\mathrm{K}^{\{l,t\}}$ are the stiffness matrices of the internal elastic forces, $\mathrm{C}^{\{l,t\}}$ are Rayleigh damping matrices with coefficients 0.1 for both mass and stiffness. $\mathbf{U}^{\{l,t\}}$ are the displacement vectors of the free nodes of the lung and the thorax respectively, $\dot{\mathbf{U}}^{\{l,t\}}$ the velocities and $\ddot{\mathbf{U}}^{\{l,t\}}$ the accelerations. $\mathbf{F}_p$ is the pressure applied to the nodes of the thorax mesh at the cavity interfaces (no pressure is applied on the other nodes). $\mathbf{F}_c^{t\to l}$ (*resp.* $\mathbf{F}_c^{l\to t}$) is the sliding interaction force generated by the thorax on the lung (*resp.* force generated by the lung on the thorax). The model is implemented in SOFA platform[2]. Equations (Eq. 1) are solved simultaneously using an implicit Euler solver (time step: $10^{-3}\,s$) and co-rotational tetrahedral finite elements to cope with large deformations and rotations [10].

Tissue Passive Properties The lungs and thorax are heterogeneous, non-linear elastic materials [7, 8]. In this first study, we want to estimate the thoracic pressure from images to simulate lung motion. Fast simulations are required as the estimation process needs several runs to converge. As a compromise, we model the lungs and thorax as homogeneous linear materials [5], with Young's moduli $\mathrm{E}^l = 900\,Pa$ and $\mathrm{E}^t = 7800\,Pa$ respectively. We can anticipate though, that regional differences in tissue stiffness will be reflected in the region-wise pressure field after optimization (Sec. 3). Poisson ratio of lungs and thorax are set according to literature values, $\nu^l = 0.4$ and $\nu^t = 0.43$ [5].

Thorax Pressure Thoracic muscles create a "negative" pressure that pulls the lung during inspiration. In our model, we apply this pressure on the surface of the thoracic cavities: $\mathbf{f}_p^i = p^i\mathbf{n}dS$, p^i is the pressure of the i-th surface zone (Sec. 2.1) and $\mathbf{n}$ is the normal of the surface element dS.

Lung/Thorax Sliding Interaction The pleural fluid in the closed inter-pleural space allows nearly friction-free lung movement. Throughout the respiratory cycle, the lung and the thoracic surfaces stay attached, which enables the thorax to control the volume of the lungs. To model this friction-free behavior, we propose a "collision" approach that does not restrict tangential sliding, but penalizes movement in the direction of the surface normals. SOFA platform provides methods to detect collisions based on proximity detection. When the distance between a vertex of a lung and a triangle of the thorax is lower than an alarm distance $\hat{d}$, a penalty constraint is added to that vertex. We modified this penalty constraint to model lung/thorax interaction, allowing friction-free sliding, but restricting inter-penetration in direction of the surface normals. Instead of applying a force that repulses two objects from each other, we apply a force that attracts two objects and whose amplitude increases with distance between the objects. Mathematically, the force generated by the

[1] www.cgal.org

[2] http://www.sofa-framework.org

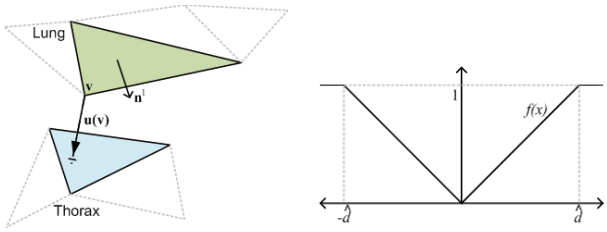


Fig. 2. *Left panel:* Drawing of the collision force, that does not restrict sliding, but penalizes inter-penetration of the thorax and lung. *Right panel:* Function that controls the amplitude of the sliding interaction force.

thorax on a vertex $\mathbf{v}$ of the lung writes (Fig. 2, left panel):

$$\begin{cases} \mathbf{F}_c^{t\to l}(\mathbf{v}) = \mathbf{0}, \text{ if } \|\mathbf{u}(\mathbf{v})\| = 0 \text{ or } \|\mathbf{u}(\mathbf{v})\| > \hat{d} \\ \mathbf{F}_c^{t\to l}(\mathbf{v}) = -\mathbf{n}^l k_s f\left(\mathbf{u}(\mathbf{v}) \cdot \mathbf{n}^l\right) \text{ otherwise} \end{cases}$$

where $\mathbf{n}^l$ is the normal vector of the triangle on the lung surface to which $\mathbf{v}$ belongs, $\mathbf{u}$ is the vector defined by $\mathbf{v}$ and the intersection point on the thorax surface (which can be anywhere on the thoracic cavity surface), k_s is the stiffness of the constraint and $f : \mathbb{R} \to \mathbb{R}$ is a damping function that controls the amplitude of the sliding interaction force as defined in Fig. 2, right panel. The interaction force generated by the lung on the thorax $\mathbf{F}_c^{l\to t}$ is defined in a similar way.

2.3. Model Personalization

The thoracic pressures necessary to deform and load the lung from EE to EI are automatically estimated using NEWUOA algorithm [11]. NEWUOA minimizes a multi-variate cost function using a trust-region method, thus avoiding the explicit calculation of the cost function gradient. This property is of particular interest for our application since our model deals with discontinuous sliding interaction forces that make the computation of the gradient prohibitive. In this study, the parameters to estimate are the pressures of every thoracic surface zone. The cost function is the mean Hausdorff distance between the simulated lung surface at system equilibrium and the segmented lung surface at EI.

3. EXPERIMENTS AND RESULTS

Data and Pre-Processing We used cases 6, 7 and 10 of the DIR-Lab dataset [12], in which the thorax was entirely visible (resolution of $0.97 \times 0.97 \times 2.50\, mm$, 11 phases). Landmarks annotated by experts were available for every phase between EI to EE (expiration). After automatic segmentation under expert supervision (Fig 1), lungs and thorax were meshed with 2819 and 30084 tetrahedron in average for the lungs and thorax respectively. We report the results on the left lung only. Non reported experiments showed that the same set up works for the right lung.

Zones	s/p	s/a	i/p	i/a	dia
Pressure (Pa)	746	439	836	469	3758

Table 1. Average pressures for superior (s), inferior (i), posterior (p), anterior (a) and diaphragmatic (dia) surfaces zones.

Case	6	7	10	Mean
Generic uniform pressure ($2500\, Pa$)				
EI surface error (mm)	12.99	16.50	15.70	15.06 ± 1.84
Optimized distributed pressures				
EI surface error (mm)	6.11	6.73	5.73	6.19 ± 0.50
EI landmark error (mm)	4.63	5.71	2.63	4.32 ± 1.56
Average landmark error during expiration (mm)	3.56 ± 1.15	3.79 ± 1.80	2.65 ± 0.55	3.33 ± 0.60

Table 2. Mean errors between simulation and ground truth.

Model Personalization and Optimization We first estimated the thoracic pressures related to the five thoracic surface zones to simulate lung loading during inspiration (from EE to EI) and minimize the effect of residual stresses on the simulated deformations. NEWUOA convergence was reached in average after 106 iterations ($\approx$ 8h on a standard computer with 4GB of memory). As anticipated, the optimal pressures (Tab. 1) reflected the different tissue properties of the thorax (modeled as a homogeneous tissue). At the interface with the diaphragm for instance, the pressure was higher to compensate for the high stiffness of our thorax model in that area. This is illustrated in Fig. 3, where one can see that applying a uniform pressure (equal to the pressure of an external ventilator) is not sufficient to correctly capture lung motion compared to optimized pressure distribution. We could thus capture different tissue properties of the thorax without changing the material coefficients. Landmark errors at EI were calculated to evaluate the inner deformation of the lung. Landmarks at EE were moved to the simulated EI phase according to the deformation of the tetrahedron to which it belongs to. Obtained landmark errors at EI ($4.32 \pm 1.56\, mm$, Tab. 2) were of the same order of magnitude as values reported in the literature, but here our model is not directly driven by image data. *Validation* We evaluated the predictive power of our model by simulating how the loaded EI lung deformed towards its EE rest state. This was performed by turning off the personalized thoracic pressures just after reaching the EI equilibrium. Simulation and images were synchronized by means of the lung volume to reproduce a real-case scenario where only exhaled air volume is available as intra-operative surrogate measurement for lung deformation prediction. Simulated landmark positions were compared with the available ground truth at every intermediate expiration phase. Despite the simplifications of our model, we obtained promising results (mean error: $3.33 \pm 0.60\, mm$) of the order of magnitude of the slice thickness (Tab. 2, Fig. 4).

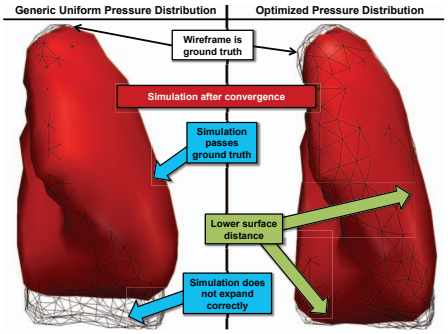


Fig. 3. Performance of optimized distributed pressure field in contrast with uniform standard pressure (see Tab. 2).

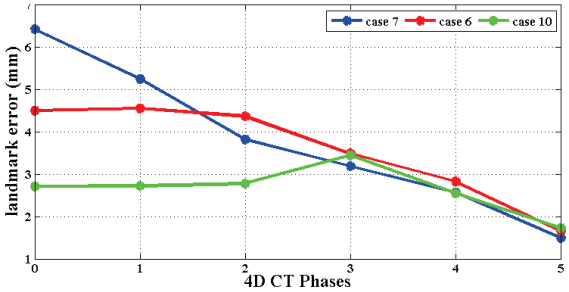


Fig. 4. Average landmark error during exhale simulation

4. DISCUSSION AND CONCLUSION

We have presented a novel approach to estimate and predict patient respiratory motion. To the best of our knowledge, our generative model is the first to simulate lung and thorax mechanics without being explicitly driven by image data. Based on pre-therapy images, the personalized model generates lung deformation using thoracic forces only, which are more directly related to intra-operative surrogates. Preliminary results are of the same order of magnitude as state-of-the-art image-driven algorithms, encouraging further works towards this direction. Uncertainties in the FEM simulation and the data can be integrated using stochastic approaches [13]. Furthermore, our method could be used to improve image reconstruction under motion in PET or CT imaging. Future work includes development of hyper-elastic model and tissue elasticity estimation [8]. Multi-resolution pressure application and additional patching of the lungs needs to be investigated to simulate spatially varying tissue properties. We are currently evaluating the performances on the other DIR-Lab datasets. In conclusion, our method may constitute a 4D surrogate tool for lung deformation prediction and therapy guidance.

References

[1] L.A. Dawson and D.A. Jaffray, "Advances in image-guided radiation therapy," *Journal of clinical oncology*, vol. 25, no. 8, pp. 938–946, 2007.

[2] E. Rietzel, G.T.Y. Chen, N.C. Choi, and C.G. Willet, "Four-dimensional image-based treatment planning: Target volume segmentation and dose calculation in the presence of respiratory motion," *IJROBP*, 2005.

[3] J. Ehrhardt, R. Werner, A. Schmidt-Richberg, B. Schulz, and H. Handels, "Generation of a mean motion model of the lung using 4d-ct image data," in *EG Workshop on VCBM*. Citeseer, 2008, pp. 69–76.

[4] T. Zhang, R. Jeraj, H. Keller, W. Lu, G Olivera, T Mackie, and B. Paliwal, "Treatment plan optimization incorporating respiratory motion," *Med. Phy.*, 2004.

[5] A. Al-Mayah, J. Moseley, M. Velec, and KK Brock, "Sliding characteristic and material compressibility of human lung: Parametric study and verification," *Med. Phy.*, vol. 36, pp. 4625, 2009, and references therein.

[6] R. Werner, J. Ehrhardt, R. Schmidt, and H. Handels, "Patient-specific finite element modeling of respiratory lung motion using 4d ct image data," *MedPhys*, vol. 36, pp. 1500, 2009.

[7] P.F. Villard, M. Beuve, B. Shariat, V. Baudet, and F. Jaillet, "Simulation of lung behaviour with finite elements: Influence of bio-mechanical parameters," in *MediVis 2005 Proceedings*. IEEE, 2005, pp. 9–14.

[8] P. Risholm, J. Ross, G. Washko, and W. Wells, "Probabilistic elastography: Estimating lung elasticity," in *IPMI*. Springer, 2011, pp. 699–710.

[9] T. Kohlberger, M. Sofka, J. Zhang, N. Birkbeck, J. Wetzl, J. Kaftan, J. Declerck, and S. Zhou, "Automatic multi-organ segmentation using learning-based segmentation and level set optimization," *MICCAI*, 2011.

[10] M. Nesme, Y. Payan, and F. Faure, "Efficient, physically plausible finite elements," *EG (short papers)*, pp. 77–80, 2005.

[11] M.J.D. Powell, "Developments of newuoa for minimization without derivatives," *IMA Journal of Numerical Analysis*, vol. 28, no. 4, pp. 649, 2008.

[12] R. Castillo, E. Castillo, R. Guerra, V.E. Johnson, T. McPhail, A.K. Garg, and T. Guerrero, "A framework for evaluation of deformable image registration spatial accuracy using large landmark point sets," *Phy. in Med. and Bio.*, vol. 54, pp. 1849, 2009.

[13] E. Konukoglu, J. Relan, U. Cilingir, B.H. Menze, N. Ayache, M. Sermesant, et al., "Efficient probabilistic model personalization integrating uncertainty on data and parameters: application to eikonal-diffusion models in cardiac electrophysiology," *Progress in BMB*, 2011.